J|A|C|S ARTICLES

Published on Web 02/10/2009

Predicting the Electrochemical Properties of MnO_2 Nanomaterials Used in Rechargeable Li Batteries: Simulating Nanostructure at the Atomistic Level

Thi X. T. Sayle,[†] R. Rapela Maphanga,[†,‡] Phuti E. Ngoepe,[‡] and Dean C. Sayle*,[†]

DASSR, Cranfield University, Defence College of Management and Technology, Shrivenham, SN6 8LA U.K., and Materials Modelling Centre, School of Physical and Mineral Sciences, University of Limpopo, Private Bag x 1106, Sovenga, 0727 South Africa

Received October 20, 2008; E-mail: d.c.sayle@cranfield.ac.uk

Abstract: Nanoporous β-MnO_2 can act as a host lattice for the insertion and deinsertion of Li with application in rechargeable lithium batteries. We predict that, to maximize its electrochemical properties, the β-MnO_2 host should be symmetrically porous and heavily twinned. In addition, we predict that there exists a "critical (wall) thickness" for MnO_2 nanomaterials above which the strain associated with Li insertion is accommodated via a plastic, rather than elastic, deformation of the host lattice leading to property fading upon cycling. We predict that this critical thickness lies between 10 and 100 nm for β-MnO_2 and is greater than 100 nm for α-MnO_2: the latter accommodates 2×2 tunnels compared with the smaller 1×1 tunnels found in β-MnO_2. This prediction may help explain why certain (nano)forms of MnO_2 are electrochemically active, while others are not. Our predictions are based upon atomistic models of β-MnO_2 nanomaterials. In particular, a systematic strategy, analogous to methods widely and routinely used to model crystal structure, was used to generate the nanostructures. Specifically, the (space) symmetry associated with the nanostructure coupled with basis *nanoparticles* was used to prescribe full atomistic models of nanoparticles (0D), nanorods (1D), nanosheets (2D), and nanoporous (3D) architectures. For the latter, under MD simulation, the amorphous nanoparticles agglomerate together with their periodic neighbors to formulate the walls of the nanomaterial; the particular polymorphic structure was evolved using simulated amorphization and crystallization. We show that our atomistic models are in accord with experiment. Our models reveal that the periodic framework architecture, together with microtwinning, enables insertion of Li anywhere on the (internal) surface and facilitates Li transport in all three spatial directions within the host lattice. Accordingly, the symmetrically porous MnO_2 can expand and contract linearly and crucially elastically under charge/discharge. We also suggest tentatively that our predictions for MnO_2 are more general in that similar arguments may apply to other nanomaterials, which might expand and contract elastically upon charging/discharging.

Introduction

Nanomaterials, in which one or more dimensions exist at the nanoscale, offer the ability to change the properties of the material or indeed proffer new properties "simply" by adjusting the size.[1] It is not surprising therefore that unprecedented efforts have focused on the synthesis,[2,3] structure,[4,5] properties,[6,7] and applications[8−10] of such materials. However, structural features that exist at the nanoscale are difficult to characterize experimentally, and therefore, atomistic computer simulation offers a unique window of exploration into such materials.[11]

In this study we develop simulation strategies for generating full atomistic models for nanomaterials, spanning all spatial dimensions including nanoparticle (0D), nanorod (1D), nanosheet (2D), and nanoporous structures (3D); such nanostructures have all been synthesized experimentally.[12−16] We illustrate the

[†] Cranfield University.
[‡] University of Limpopo.

(1) Rodriguez, J. A. *Synthesis, Properties and Applications of Oxide Nanomaterials*; Rodriguez, J. A., Garcia M. F., Eds.; John Wiley & Sons, Inc.: Hoboken, NJ, 2007.
(2) Pinna, N.; Niederberger, M. *Angew. Chem., Int. Ed.* **2008**, *47*, 5292–5304.
(3) Lai, M.; Riley, D. J. *J. Colloid Interface Sci.* **2008**, *323*, 203–212.
(4) Thomas, J. M.; Midgley, P. A. *Chem. Commun.* **2004**, *11*, 1253–1267.
(5) Möbus, G.; Inkson, B. J. *Mater. Today* **2007**, *10*, 18–25.
(6) Lai, M.; Kulak, A. N.; Law, D.; Zhang, Z. B.; Meldrum, F. C.; Riley, D. J. *Chem. Commun.* **2007**, *34*, 3547–3549.
(7) Hahn, H. *Adv. Eng. Mater.* **2003**, *5*, 277–284.
(8) Feng, X. D.; Sayle, D. C.; Wang, Z. L.; Paras, M. S.; Santora, B.; Sutorik, A. C.; Sayle, T. X. T.; Yang, Y.; Ding, Y.; Wang, X. D.; Her, Y. S. *Science* **2006**, *312*, 1504–1508.
(9) Berry, C. C. *J. Mater. Chem.* **2005**, *15*, 543–547.
(10) Tarnuzzer, R. W.; Colon, J.; Patil, S.; Seal, S. *Nano Lett.* **2005**, *5*, 2573–2577.
(11) Sayle, D. C.; Seal, S.; Wang, Z.; Mangili, B. C.; Price, D. W.; Karakoti, A. S.; Kuchibhatla, S. V. T. N.; Hao, Q.; Mobus, G.; Xu, X.; Sayle, T. X. T. *ACS Nano* **2008**, *2*, 1237–1251.
(12) Debart, A.; Paterson, A. J.; Bao, J.; Bruce, P. G. *Angew. Chem., Int. Ed.* **2008**, *47*, 4521–4524.
(13) Zhou, Q.; Li, X.; Li, Y. G.; Tian, B. Z.; Zhao, D. Y.; Jiang, Z. Y. *Chin. J. Chem.* **2006**, *24*, 835–839.
(14) Jiao, F.; Bruce, P. G. *Adv. Mater.* **2007**, *19*, 657–660.
(15) Matsumoto, Y.; Ida, S.; Inoue, T. *J. Phys. Chem. C* **2008**, *112*, 11614–11616.
(16) Li, G. R.; Qu, D. L.; Yu, X. L.; Tong, Y. X. *Langmuir* **2008**, *24*, 4254–4259.

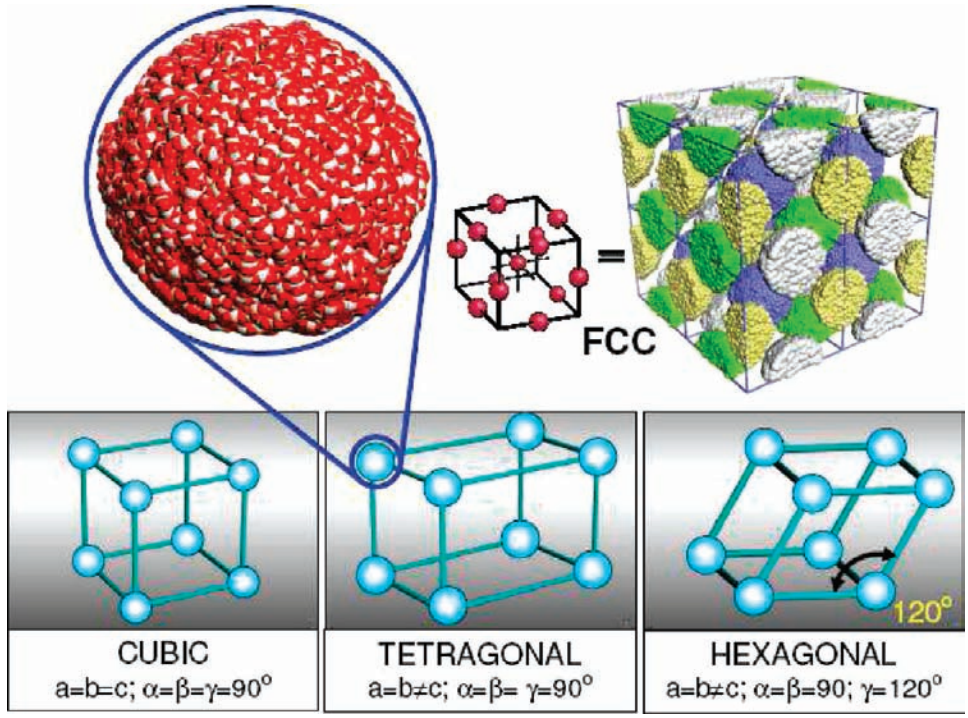

Figure 1. Schematic illustrating the systematic construction of a nanostructure. Possible simulation cells, for example, cubic, tetragonal, hexagonal, are shown below, and a nanoparticle is positioned at basis positions to conform to a particular space group. Top right shows nanoparticles positioned in a face centered cubic array.

Table 1. Dimensionality, Simulation Duration, Cell Sizes, Densities, and Wall Thicknesses Pertaining to Each of the Nanostructures

dimension	name	simulation time (ns)	simulated cell size (nm^3)	density (cm^3/g)	wall thickness (nm)
0D	particle	25	$10.0 \times 10.0 \times 10.0$		8
1D	rod	21	$10.0 \times 8.5 \times 10.0$		6
2D	sheet	25	$8.5 \times 8.5 \times 8.5$		3−6
3D	porous	27	$7.4 \times 7.4 \times 7.4$	0.341	4−7
	bulk	25	$6.3 \times 6.3 \times 6.3$	0.210	

approach by generating nanostructural models of MnO_2, an important material with respect to energy storage. Indeed, "rechargeable lithium batteries have revolutionized portable electronic devices".[17] However, to facilitate viable electric vehicles, one needs to increase both the energy density and discharge rates. One avenue of exploration in achieving such goals is the use of nanomaterials. For example, Jiao and Bruce found that mesoporous β-MnO_2 is capable of reversibly storing 284 mA h g^{-1}, which corresponds to $Li_{0.92}MnO_2$. Conversely, bulk β-MnO_2 can accommodate very little Li on electrochemical discharge. The authors attributed this to the ability of the mesoporous walls to accommodate the volume changes associated with charging and discharging. In addition, the high contact area of the electrolyte with the porous surface together with the short diffusion distance of the Li^+ (wall thickness 7 nm) facilitates high charge/discharge rates.

Such exemplary and complementary properties for both storage and discharge rates suggest that one should explore nanomaterials further as materials, which can potentially facilitate step changes in storage and discharge rates.[14] Moreover, if we can better understand the phenomenon and characterize those mechanisms associated with storage and discharge, then we can design intelligently new (nano)materials with optimized properties. Ultimately, such endeavors will enable us to realize viable electric vehicles. However, the important chemistry facilitating charge/discharge occurs deep within the framework architecture of the MnO_2, a region notoriously difficult to probe experimentally.[4] Accordingly, atomistic computer simulation is well positioned to help experiment because it can provide insights, at the atomistic level, pertaining to such structures. Here the challenge is to create models that capture adequately the structural complexity within a real nanomaterial such that the model can be used to characterize the structure and simulate important processes with sufficient accuracy to be of benefit to experiment.

Jiao and Bruce found that mesoporous β-MnO_2, with wall thicknesses of about 7 nm, facilitated exemplary properties with respect to energy storage in rechargeable Li batteries; the bulk β-MnO_2 was not found to proffer similar attributes.[14] Here, we use this study, together with similar experimental data on mesoporous MnO_2 by Zhou and co-workers,[13] to help direct and validate the generation of full atomistic models for nanomaterials. We then use the atomistic models to help explain the experimental observations.

Simulation Strategy. Most atomistic simulation methodologies proceed by utilizing the symmetry of the system, together with the coordinates of the basis atoms, to generate a crystallographic array, periodic in three dimensions.[18] Indeed, this strategy, which enables one to systematically prescribe the structure of (almost) any crystal, has been widely used for over 60 years.[19,20] The obvious success of this strategy advocates using an analogous approach to model nanomaterials. Accordingly, we utilize the

(17) Bruce, P. G.; Scrosati, B.; Tarascon, J. M. *Angew. Chem., Int. Ed.* **2008**, *47*, 2930–2946.

(18) Gale, J. D. *Z. Kristallogr.* **2005**, *220*, 552–554.
(19) Mott, N. F.; Littleton, M. J. *Trans. Faraday Soc.* **1938**, *34*, 485.
(20) Lidiard, A. B. *J. Chem. Soc., Faraday Trans. 2* **1989**, *85*, 341–349.

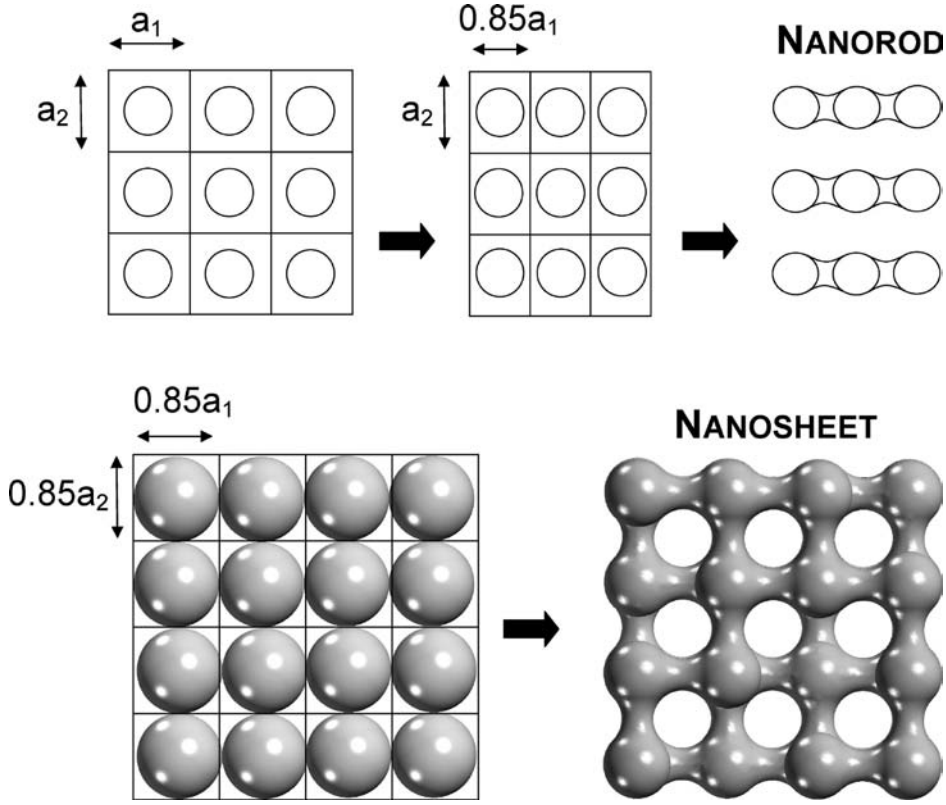

Figure 2. Schematic illustrating the strategy used to construct extended nanostructures. Top: a periodic array of nanoparticles is constructed in which the nanoparticles are introduced into simulation cells of size $a_1 \times a_2$. The simulation cell sizes are then reduced to $0.85a_1 \times a_2$, top middle. The close proximity between nanoparticles along a_1 causes the nanoparticles, under MD, to start to agglomerate, top right, facilitating the evolution of a one-dimensional nanorod. On the other hand, if the sizes of the simulation cells are reduced to $0.85a_1$ and $0.85a_2$, bottom left, the nanoparticles can agglomerate in two directions facilitating the evolution of a nanosheet, bottom right. If the nanoparticles agglomerate in all three directions, a porous architecture results. Clearly, if distance between neighboring nanoparticles is high, then the nanoparticles are not able to agglomerate.

(space) symmetry of the mesoporous material and position model nanoparticles at basis positions. This strategy, which we outlined previously,[10] enables one to systematically prescribe an atomistic model for a nanomaterial in a similar way that one can generate routinely an atomistic model for a particular crystal structure. Here, we test the strategy: we validate it against available experimental data and then use it predictively to aid experiment in an area where experimentation to provide insight is difficult or intractable.

Experimentally, Zhou and co-workers impregnated a mesoporous silica template, KIT-6, with a saturated $Mn(NO_3)_2$ solution.[13] The system was heated to 400 °C (crystallized) and the template dissolved. The resulting MnO_2 nanostructure retained the symmetry (*Ia3d)* of the silica template. In addition, the MnO_2 exhibited the pyrolucite polymorph, β-MnO_2.

An atomistic model for this nanostructure can be generated by constructing a simulation cell with lattice parameter in accord with experiment (24.6 nm) and positioning nanoparticles at basis positions to facilitate *Ia3d* symmetry; periodic boundary conditions replicate the material infinitely in three (bulk) or two (surface) dimensions. Under MD simulation, the amorphous nanoparticle will agglomerate with its periodic neighbors to formulate the walls of the nanomaterial.[10] The size of the nanoparticle can be adjusted to enable the wall thicknesses of the model to accord with the wall thickness of the real material. A schematic of this process is shown in Figure 1.

In this study, the computational facilities required to generate such a model would far outweigh those available. Accordingly, we captured the (cubic) symmetry of the nanostructure by constructing a simulation cell with cubic symmetry and positioned a MnO_2 nanoparticle centered at lattice points of the primitive cubic Bravais lattice; periodic boundary conditions were used to replicate the structure infinitely in three dimensions. The amorphous nanoparticle was then agglomerated with its periodic neighbors to facilitate the pore structure including cavities and connecting channels. Finally, the polymorph of the MnO_2, together with a variety of microstructural features, was evolved using simulated crystallization. This strategy, similar to experiment, enables the symmetry of the pore architecture to influence the particular polymorph and microstructural features. This is likely to facilitate a more realistic model because it negates the need to predefine (perhaps artificially) the structure.

Method

Potential Models and Simulation Code. The Born model of the ionic solid was used to describe the MnO_2 in which the component Mn and O ions interact via short-range parametrized interactions coupled with long-range Coulombic interactions. The parameters, which have been published previously,[21] reproduce the lattice parameters for pyrolusite and ramsdellite to within 3% and 4%, respectively, of experimentally determined values and predict, in agreement with experiment, that pyrolusite is energetically more stable than ramsdellite. The DL_POLY code,[22] which imposes 3D periodic boundary conditions, was used to perform all the Molecular Dynamics (MD) simulations in this study.

(21) Sayle, T. X. T.; Catlow, C. R. A.; Maphanga, R. R.; Ngoepe, P. E.; Sayle, D. C. *J. Am. Chem. Soc.* **2005**, *127*, 12828–12837.

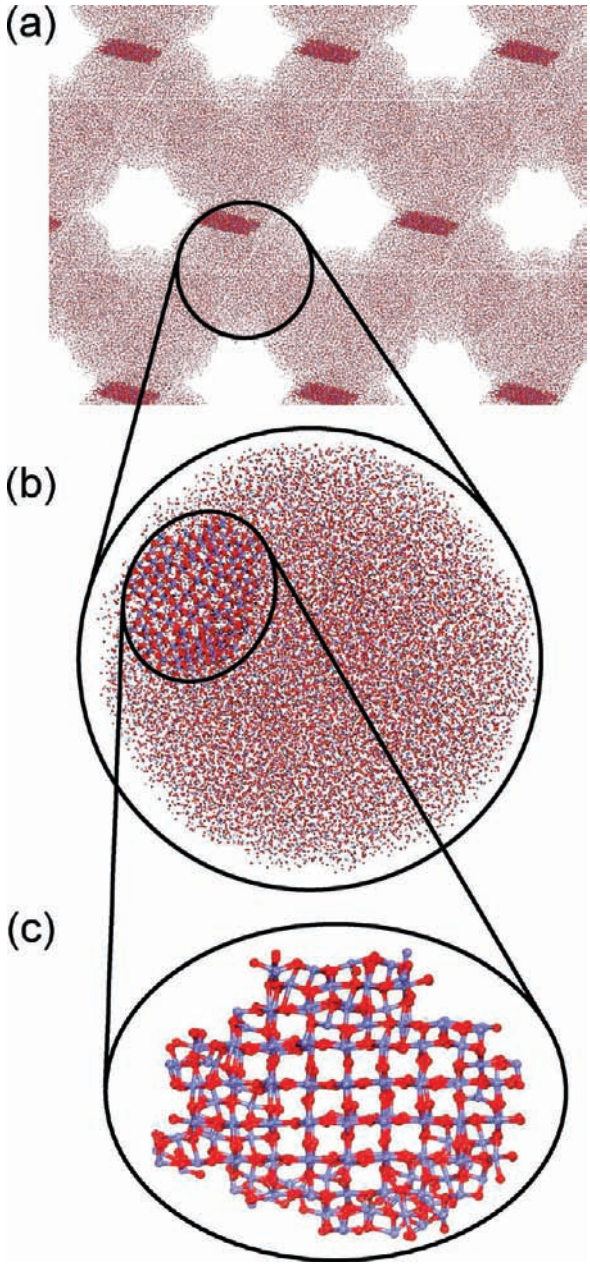

Figure 3. Atomistic models for the nanoporous MnO_2 depicting the nucleating seed, which facilitates crystallization of the nanomaterial: (a) view looking along [111] of the nanostructure; (b) enlarged view of a nanoparticle, which comprises the nucleating seed; (c) enlarged view of the nucleating seed revealing more clearly its atomistic structure, which conforms to the pyrolusite polymorph and is isostructural with rutile, TiO_2.

Generation of Structural Models. The first step was to generate the amorphous nanoparticle, which was then positioned at basis positions to facilitate the desired nanostructure. To this end, a cube of MnO_2 comprising 24696 atoms was cut from the parent (bulk) material. Tension induced amorphization[23] of the nanoparticle was achieved by increasing the lattice parameter of the nanoparticle by +36.3% and applying MD simulation at 2000 K for 750 ps. Under these conditions, the MnO_2 nanoparticle spontaneously amorphized; radial distribution functions (not shown) revealed that the nanoparticle had lost all long-range order, indicative of an amorphous material.[24]

To facilitate the variety of different nanostructures, the simulation cell size, Table 1, was adjusted to enable neighboring nanoparticles to agglomerate. For example, for a nanoparticle (0D), one does not wish neighboring nanoparticles to agglomerate. Accordingly, the size of the simulation cell was maintained sufficiently high (in all dimensions) to prevent neighboring nanoparticles from first attracting one another and then agglomerating upon contact. To facilitate a nanorod, the simulation cell was reduced in one dimension to enable neighboring nanoparticles to agglomerate in one direction, thus facilitating a rod. A schematic is shown in Figure 2. Agglomeration of neighboring nanoparticles in two and three dimensions facilitates nanosheets and nanoporous architectures, respectively. To facilitate a model for the bulk material, the simulation cell size was reduced such that the atoms, comprising the amorphous nanoparticle, filled the simulation cell with no void

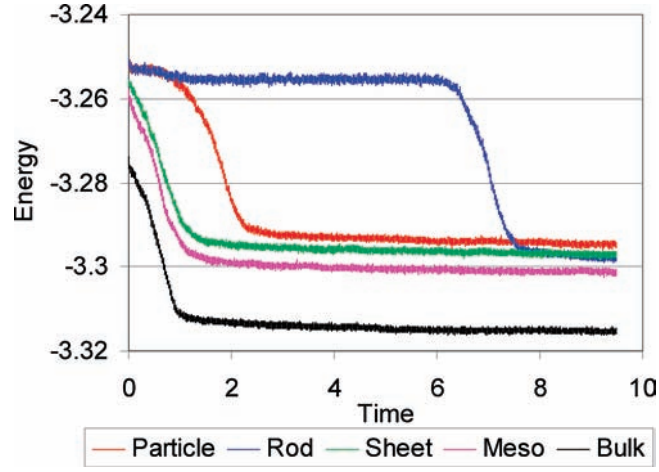

Figure 4. Configuration energy (10^5 eV) calculated as a function of time (ns) for each of the nanostructures. The abrupt change in energy reflects a phase change and is associated with the amorphous−crystalline transition; the difference in energy between the starting (amorphous) configuration and the final (crystalline state) reflects loosely the heat of crystallization. Note the extraordinary time required to crystallize the nanorod. This was attributed to the reamorphization of the nucleating seed and the time required to (spontaneously) evolve a new nucleating seed.

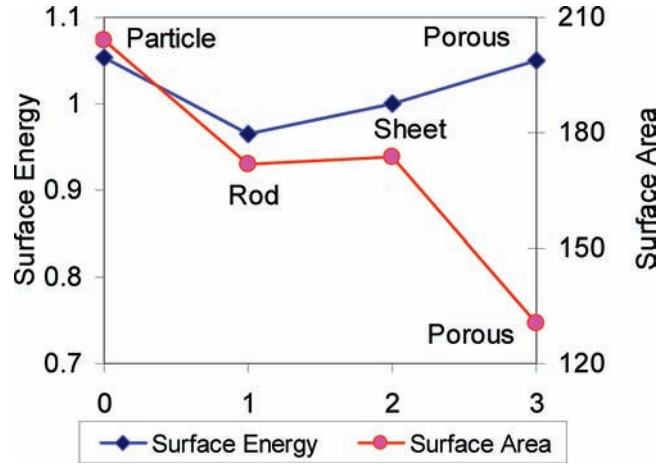

Figure 5. Surface energy (left ordinate, J m^{-2}) and surface area (right ordinate, m^2 g^{-1}) calculated for each of the four nanostructures as a function of dimensionality: 0D nanoparticle, 1D nanorod, 2D nanosheet, and 3D nanoporous structure.

(22) *DL_POLY* is a package of Molecular Simulation routines written by Smith and Forester, copyright by the council for the Central Laboratory of the Research Councils. Smith, W.; Forester, T. R. *DL_POLY*; Daresbury Laboratory: Daresbury, Warrington, U.K., 1996; http://www.dl.ac.uk/TCSC/Software/DLPOLY.

(23) Sayle, T. X. T.; Parker, S. C.; Sayle, D. C. *Chem. Commun.* **2004**, *21*, 2438–2439.

(24) Sayle, D. C.; Watson, G. W. *Surf. Sci.* **2001**, *473*, 97–107.

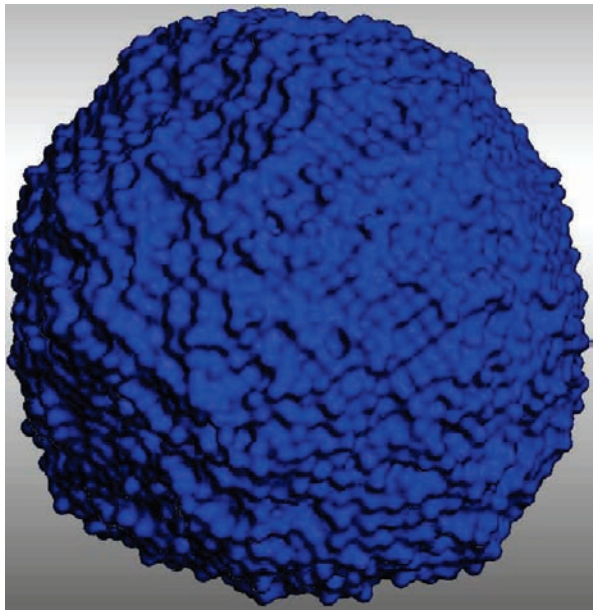

Figure 6. Surface rendered model of the MnO_2 nanoparticle revealing its spherical morphology.

space. This was achieved, by applying constant pressure MD simulation with a 10 GPa pressure; similar to a liquid, the amorphous MnO_2 material under MD simulation, fills the simulation cell completely. Finally, each system was crystallized by performing constant volume MD simulation at 2000 K for a duration sufficient to ensure that the nanostructures were no longer changing structurally or energetically.

A major developmental challenge associated with this work was the successful crystallization of each of the nanostructures. In particular, under MD simulation, an amorphous seed must *spontaneously* evolve to nucleate crystallization of the amorphous material. The time required for evolution for such a seed can be considerable (in terms of CPU usage). Accordingly, we performed MD simulation on the isolated nanoparticle (building block) until a nucleating seed evolved. This amorphous nanoparticle, which included a nucleating seed, was used as the "basis" nanoparticle for constructing all the other nanostructures. The strategy is best communicated in Figure 3. With careful inspection of the nucleating seed, Figure 3c reveals it conforms to the β-MnO_2 polymorph; the degree of amorphicity increases as one moves radially from the center of the seed. In particular, the transition from crystalline to amorphous does not appear abrupt; rather as one moves from the center of the seed to the outside one can start to see the structure become more disordered.

Results

The configurational energy of each system, calculated as a function of time, is shown in Figure 4, which reveals complete crystallization for "bulk", "nanosheet", and "nanoporous" architectures after about 1−2 ns. Conversely, crystallization of the nanoparticle and nanorod occurred after 3 and 8 ns, respectively.

Surface Area, Surface Energy, and Stability. The calculated surface energies and surface areas for each of the four nanostructures are shown in Figure 5. The abscissa refers to the dimensionality of the nanostructure: particle (0D), rod (1D), sheet (2D), and porous structure(3D).

Calculated surface areas of the MnO_2 nanostructures decrease in the order nanoparticle > nanorod ≈ nanosheet > nanoporous structure. Clearly, for real materials, the (nano)particles, rods, and sheets would likely be in contact; our calculations have been made assuming that there is no contact between neighboring nanostructures. Accordingly, calculated surface areas (apart from the nanoporous structure) are likely overestimated compared with experiment. Measurements on mesoporous MnO_2, synthesized by Yuan and co-workers,[13] revealed a Brunauer−Emmett−Teller specific surface area of 118 $m^2\ g^{-1}$, wall thickness of 9.7 nm, and volume of 0.35 $cm^3\ g^{-1}$. Our structural models, Table 1, are in accord with these values. Measurements on MnO_2 nanorods[12] revealed surface areas of 12 $m^2\ g^{-1}$, much lower than our calculated values. However, we note that the nanorods were about 80 nm in diameter, which are about 10 times larger than our models.

It can be argued that the stability of the nanostructures should align with the surface area because surface exposure is energetically unfavorable. Indeed, the calculated relative stabilities of the nanostructures follow (surface energies reflect the energy required to facilitate the surface; accordingly, the higher the surface energy the less stable the surface): particle < sheet < rod. However, the porous nanostructure is more unstable than one might have predicted. This can be attributed to structural features, other than surface area, that will impact strongly upon the stability. Factors will likely include the following: the surface morphology (specific surfaces exposed) and curvature. Rods and particles expose wholly convex surfaces, whereas sheets and porous architectures expose both convex and concave surfaces. The degree of (micro)twinning is also significant; grain boundaries are defects and are therefore deleterious to the stability of the system. The nanostructures also comprise point defects[25] such as vacancies; ionic relaxation is also extensive for such complex structures, especially those that comprise high surface curvatures.

Clearly, the nanostructures are metastable compared with the parent bulk material. On the other hand, these materials are capable of maintaining (desirable) metastability throughout their useful application lifetime; Jiao and Bruce showed that they can cycle many times with no loss of structure.[14,17] Moreover, Lai and co-workers found that ordered nanoporous materials were mechanically more durable compared to irregular nanoporous materials[6] because they can respond elastically, rather than plastically, over a wider range (%) of mechanical deformation.

Structural Considerations. When used as a rechargeable battery material, the host MnO_2 must undergo charge/discharge cycling, where Li^+ species are, respectively, deinserted/inserted into the MnO_2 lattice without structural modification. Clearly, to glean insight into this process and help understand how the host lattice can maintain structural integrity under cycling, one desires to understand how the Li^+ species enter the host. Equipped with a structural (atomistic) model, one can explore this process computationally. Conversely, it is very difficult to extract such insight, deep within the nanostructure, using experiment. To this end we explore all the nanostructures using graphical techniques.

(0D) Particle. The atomistic structure of the MnO_2 nanoparticle is shown in Figure 6, which reveals a spherical morphology. The MnO_2 crystallizes into the β-MnO_2 structure in accord with experiment. We note that this polymorph was not imposed upon the structure; rather, the model structure was allowed to crystallize into any polymorph it desired, driven by the potential model describing the ionic interactions rather than any (perhaps erroneous) decision to impose any particular polymorph. Similar

(25) Harding, J. H. *Rep. Prog. Phys.* **1990**, *53*, 1403–1466.

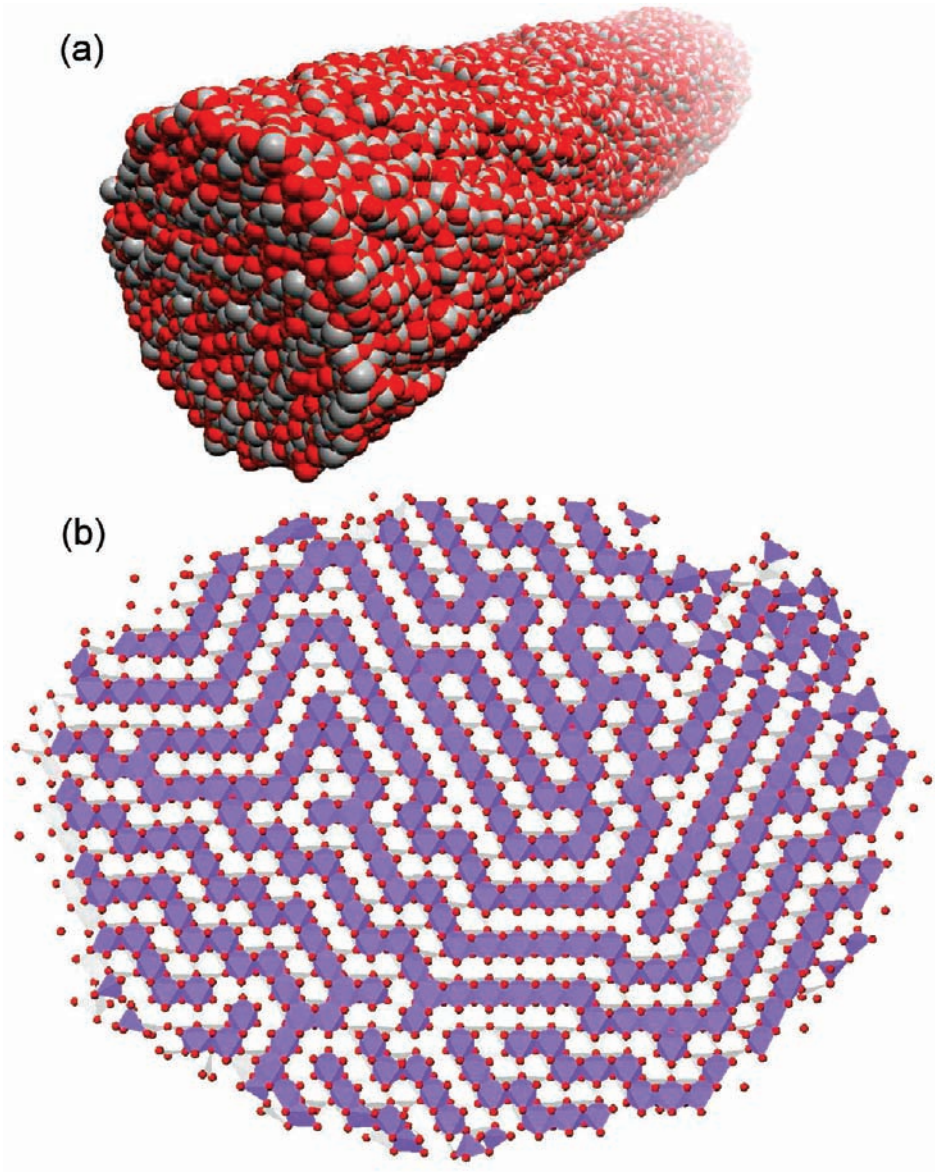

Figure 7. Morphology and microstructure of the MnO_2 nanorod: (a) sphere model representation of the atom positions comprising the nanorod (oxygen is colored red and manganese is gray), and (b) slice cut through the nanorod revealing the MnO_2 conforms to the pyrolusite polymorph and undergoes considerable microtwinning. Note the shape of the slice is not circular. This is because the planes of Mn and O (and hence the cut slice) are not normal to the length of the rod.

to the nanoparticle, the other nanostructures all crystallized into the β-MnO_2 polymorph.

(1D) Rod. The atomistic structure of the MnO_2 nanorod is shown in Figure 7. Inspection of the surface of the rod does not reveal any obvious faceting or exposure of particular (low energy) surfaces. A slice cut through the rod, Figure 7b, reveals considerable microtwinning of the lattice. We also note vacancies in the nanoparticle.

(2D) Sheet. The atomistic structure of the MnO_2 nanosheet is shown in Figure 8. Inspection of the model reveals that the nanostructure exposes both concave and convex surfaces with some evidence of faceting including surface steps, edges, and corners. It is difficult to assign a particular index to the surface because of the small area and high (positive and negative) curvature of the nanosheet.

(3D) Porous. In Figure 9a−c, a slice cut through the nanoporous material at the start of the simulation is shown; the MnO_2 is still amorphous at this point. The structure reveals clearly that the architecture comprises positive curvature (convex) of the material, derived from the spherical building blocks. However, under MD simulation the nanoparticles start to agglomerate and the ions move in an attempt to minimize the surface energy. After 12 ns, Figure 9d−f, the framework structure reveals a concave morphology. Essentially, a minimal surface evolves. A schematic of this process is communicated in Figure 9c,f.

In Figure 10 the final, 0K, structure for the porous MnO_2 model is shown; a slice cut through the nanoporous MnO_2 oriented with [111] normal to the plane of the page reveals a hexagonal array of channels. A perspective view, Figure 10b, reveals more clearly the nanoporous architecture of the model, which comprises cavities interconnected by channels. The MnO_2 model comprises crystalline walls, Figure 10c,d. Comparison between experiment, Figure 10e,f, and the model structure reveals that the model captures the basic architectural features of nanoporous MnO_2.

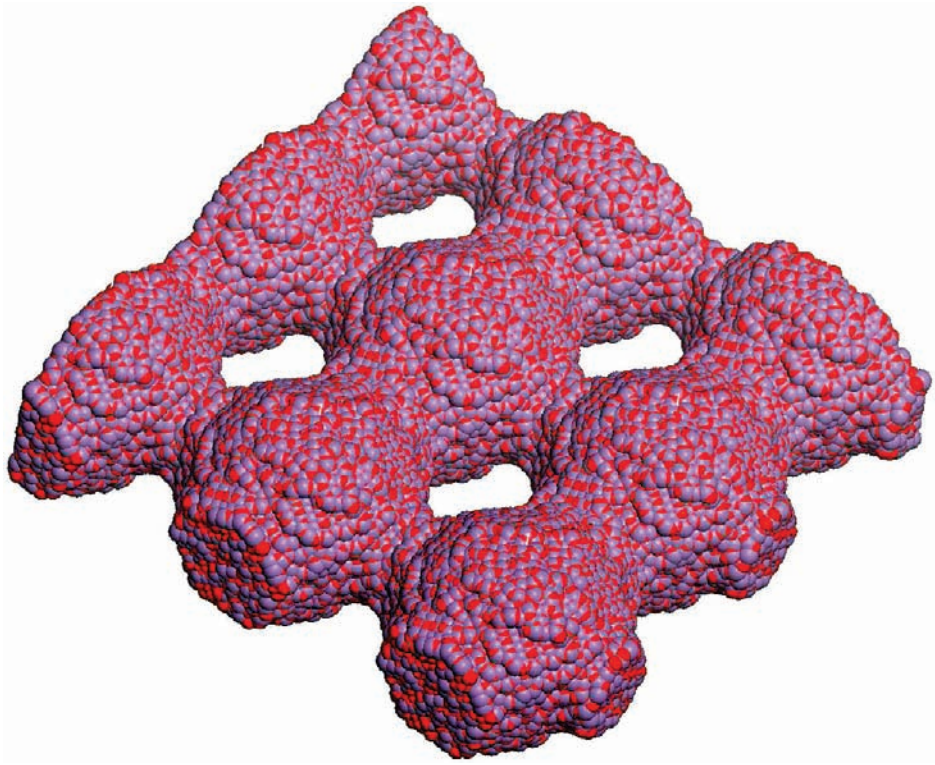

Figure 8. Sphere model representation of the atom positions comprising the MnO_2 nanosheet. Oxygen ions are colored red and manganese are blue.

The XRD, calculated for the nanoporous material, Figure 11b, is in full accord with experiment, Figure 11c. The peaks have broadened considerably (experiment and calculated) compared with the calculated XRD associated with the perfect parent bulk material, Figure 11a. We attribute this to the considerable microtwinning within the material.[26]

Clearly, an atomistic model is of little value if it simply confirms what experiment already knows; rather, the power/value of the simulation is in its predictive capability. Thus far, we have simply validated the models. The close analogy between experiment and model at three levels of hierarchical structural complexity, crystal structure (β-MnO_2 polymorph), microstructure (microtwinning and point defects), and nanostructure (particle, rod, sheet, porous structure), enables us to have confidence in using the models predictively.

Predictions. To understand how the porous MnO_2 can facilitate Li cycling and maintain structural integrity, we explore the (internal) surfaces of the material. To this end the model has been drawn in various length scales in Figure 12. In part a, an extended region of the nanoporous MnO_2 architecture is shown; a small segment of this is enlarged in part b to reveal the repeat unit. If one then magnifies a region of the internal surface (part c), one can see the (1×1) tunnels that the Li must insert into; a schematic of the tunnel is shown in part d.

Figure 13a shows a perspective view inside a cavity within the nanoporous MnO_2: one can clearly see the cavity and interconnecting channels. Clearly, the Li needs to insert into the internal surface of the nanomaterial; Li ions, colored yellow, are show as schematics to illustrate. To understand better this process, we need to explore the internal surface. To this end a slice was cut through the MnO_2 and is shown in Figure 13b. Here, two layers of Mn ions (parallel to the plane of the page) are shown as white or blue polyhedra; the microtwinning of the MnO_2 is clearly evident. In part c, an enlarged segment of part b is shown revealing that the Li ions can insert into the nanoporous MnO_2 via 1×1 tunnels at a variety of positions on the internal surface, facilitated by the considerable microtwinning; Li ions, colored yellow, are included on the image as schematics. Without such microtwinning we hypothesize that the Li would insert only in one dimension (*c*-direction, along the 1×1 tunnels) as transport along *b*- and *c*-directions is blocked.

In Figure 14a an enlarged segment of Figure 13b is shown. Two Li ions (schematic), colored yellow, indicate a path that the Li might take once inside the MnO_2. Notice it changes direction at the microtwin boundary. At the end (direction of the arrow) it appears the tunnel is blocked by a Mn ion. However, further analysis using molecular graphics revealed that the tunnel was not blocked; rather the "blockage" is actually another twin boundary that is not in the plane of the page. Accordingly, by inspection of the structure we can observe that the Li ion is free to insert at many positions on the internal surface and can move in all three spatial directions once inside the nanoporous material; a schematic is depicted in Figure 14b to better communicate Li transport in the nanostructure.

Calculated Radial Distribution Function (RDF) for each of the five nanostructures (not shown) reveal nearest neighbor Mn−O distances of 1.88 Å in accord with experiment. Nearest neighbor distances range from 1.75−2.00 Å, which reflects the considerable ionic relaxation.

Discussion

Elastic−Plastic Transition. Nanoporous MnO_2, when used as a host lattice in a rechargeable battery, can undergo many charge/discharge cycles while maintaining its structural inte-

(26) Sayle, T. X. T.; Catlow, C. R. A.; Maphanga, R. R.; Ngoepe, P. E.; Sayle, D. C. *J. Cryst. Growth* **2006**, *294*, 118–129.

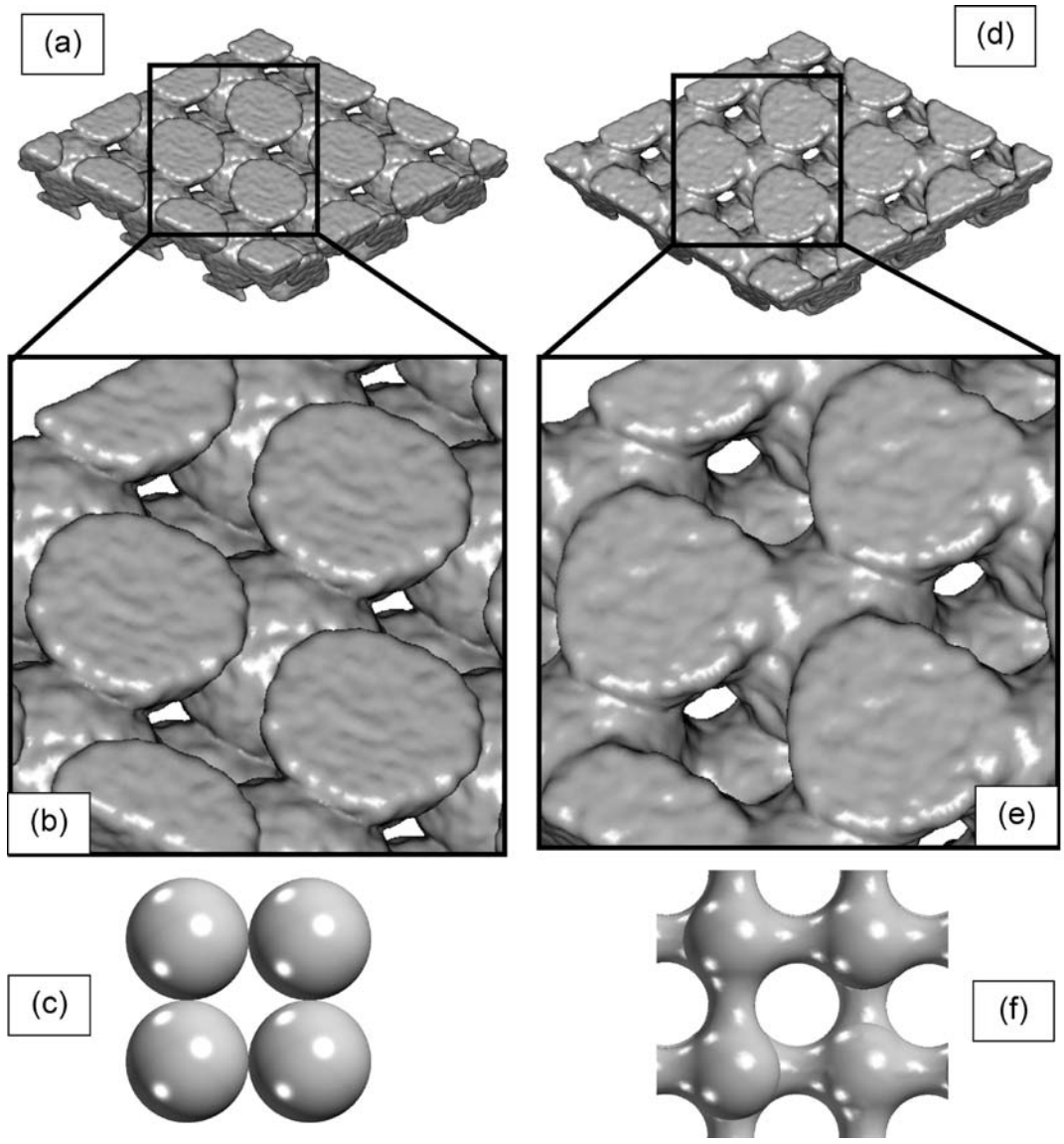

Figure 9. Evolution of the nanoparticles into the walls of the nanostructure. Top: slice cut through the nanostructure viewing along [111]: (a) starting structure, (d) after 12 ns. Middle (b and e): enlarged view of parts a and d, respectively. Bottom: schematics of the process showing how material comprising the nanoparticle can agglomerate with a neighboring nanoparticle to facilitate a wall.

grity.[14,17] Conversely, the parent bulk material does not proffer such properties; rather the latter material deforms structurally upon Li insertion.[14] This behavior was attributed, by the authors, to the ability of the nanoporous architecture to "expand into the pores".

Building upon this argument, we propose that the porous host architecture is able to deform elastically, rather than plastically, during cycling: Jiao and Bruce found that the lattice parameter of the porous β-MnO_2 changes from $a = 4.40$ Å, $c = 2.88$ Å to $a = 5.01$ Å, $c = 2.81$ Å upon insertion.[14] Specifically, Li, when introduced (at concentration levels commensurate with those used experimentally) into the surface of the parent bulk β-MnO_2, would change the lattice parameter of the uppermost surface layer from 4.40 to 5.01 Å (6.5%). This strain can likely be accommodated for a single "layer", the energy associated with maintaining favorable (cation−anion) interactions far outweighing the energy required to strain the surface layer. However, as the insertion continued, Li would percolate deeper into the surface. To maintain a coherent interface, each successive layer would need to be strained. Indeed, the strain energy is additive for each successive layer. Conversely, the energy returned to maintain a coherent interface remains constant. Accordingly, we argue that at some particular "critical thickness" the strain energy will outweigh the interaction energy and the system will facilitate strain relaxation via a plastic structural transformation (for supported heteroepitaxial thin films this is typically via dislocation evolution).

We predict that there exists a critical thickness pertaining to the elastic−plastic deformation for host lattices. Further supporting evidence comes from Débart and co-workers who find that the energy storage capacities of nanorods of β-MnO_2, 100 nm in diameter, fade very rapidly upon cycling, which indicates a plastic rather than elastic deformation upon cycling. Accordingly, on the basis of this experimental data, we predict that the critical thickness lies between 10 and 100 nm. We note that the bulk crystalline β-MnO_2 converts to $LiMn_2O_4$ spinel on chemical intercalation.[14] In addition, Tang and co-workers find that the "lithium insertion behavior in

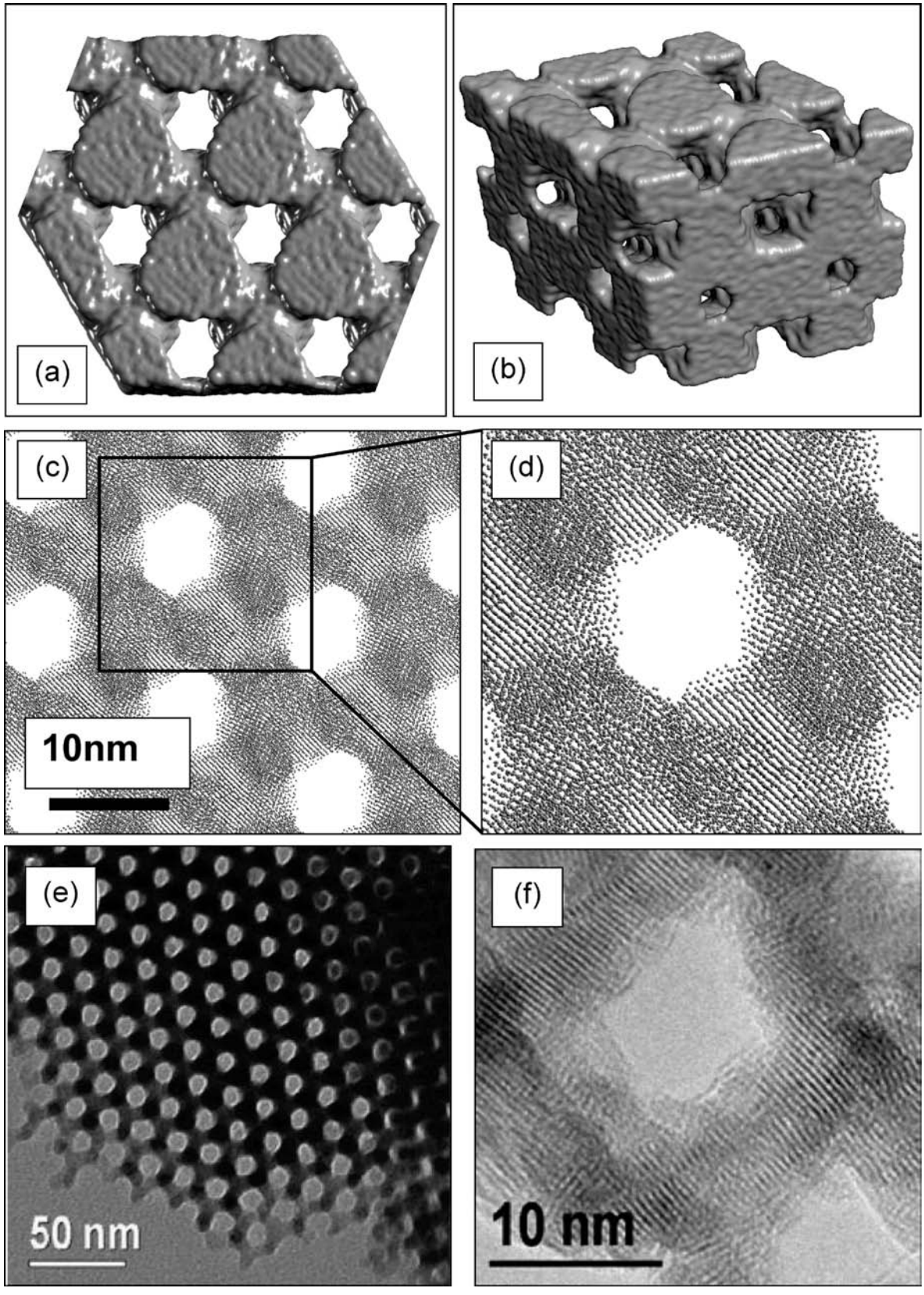

Figure 10. Final, low-temperature structures compared with experiment: (a) surface rendered model of a thin slice viewed along [111]; (b) perspective view of a surface rendered model of the nanostructure; (c) sphere model representation of the atom positions revealing the hexagonal array of channels and the atomic planes of the MnO_2; (d) enlarged view of part c; (e) TEM; (f) high-resolution TEM of nanoporous MnO_2 taken from reference 14, copyright 2007 Wiley-VCH Verlag GmbH and Co. KGaA. Reproduced with permission.

the first discharge process depends strongly upon the size of the β-MnO_2 nanocrystals".[27]

Further evidence is presented by Debart and co-workers, who find that, in contrast to β-MnO_2 nanorods, α-MnO_2 nanorods

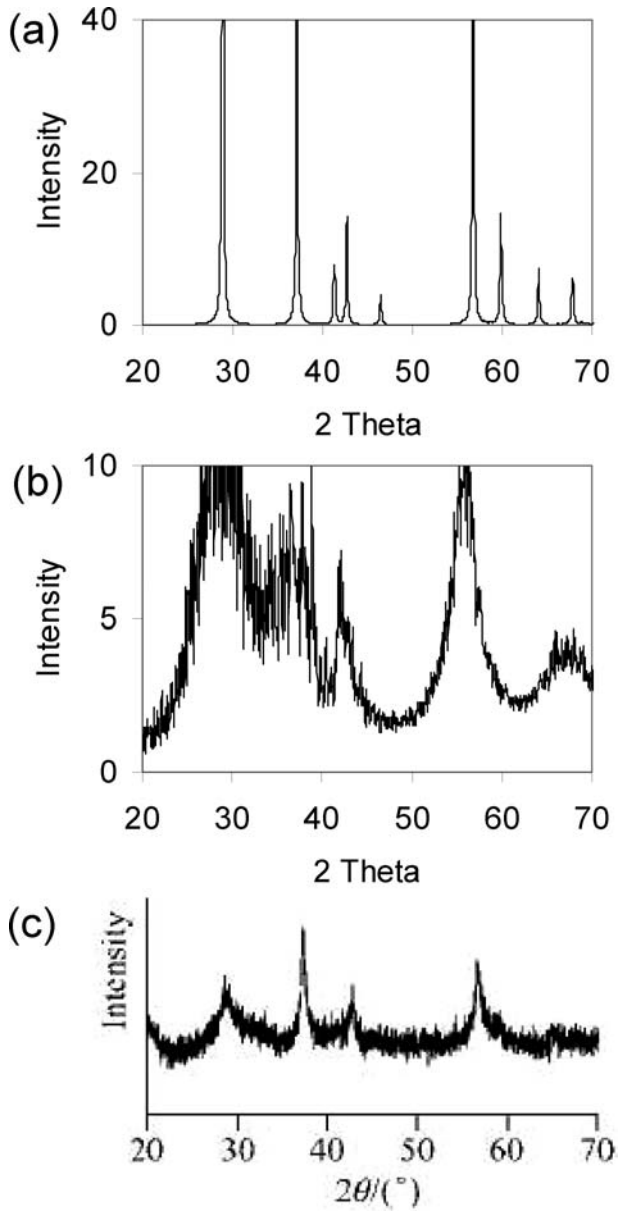

Figure 11. Calculated XRD for nanoporous MnO_2 compared with experiment: (a) pure β-MnO_2 (model); (b) nanoporous MnO_2 (model); (c) nanoporous MnO_2, reproduced from reference 13, copyright 2006 Wiley-VCH Verlag GmbH and Co. KGaA. Reproduced with permission.

with ca. 100 nm diameters enjoy good capacity retention upon cycling. We attribute this to the larger size of the tunnels: α-MnO_2 comprises 2 × 2 tunnels compared with the 1 × 1 tunnels found in β-MnO_2. Here, we predict that for α-MnO_2 the critical thickness to plastic deformation is above 100 nm.

The authors also advocate restricting the depth of discharge to maintain the exemplary electrochemical properties during cycling, which provides compelling evidence to support the idea that retention of the electrochemical properties is achieved by elastic deformation of the lattice. For example if Li were introduced into all available sites (deep discharge), the stress would be much higher than if Li were introduced into only, for example, 20% of available sites along the 1 × 1 tunnels. This experimental data indicates that the critical

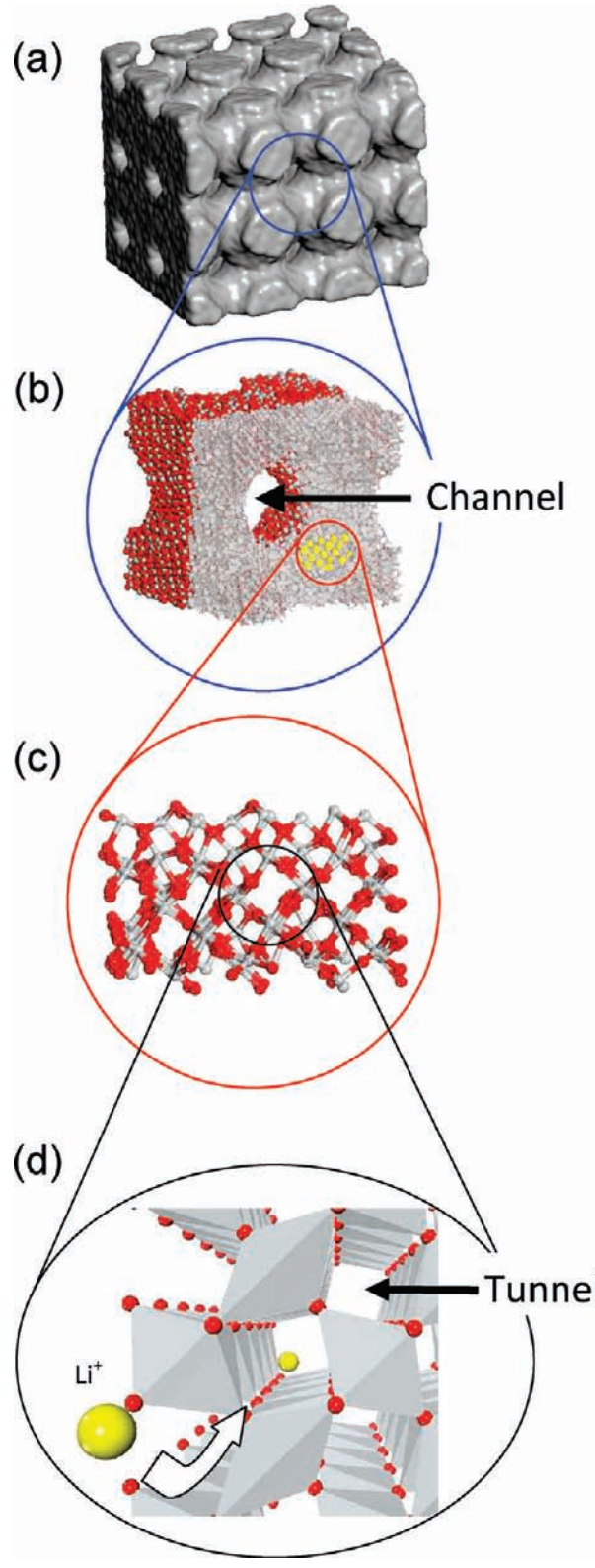

Figure 12. Hierarchical model structure of nanoporous MnO_2: (a) surface rendered model showing the porous structure, (b) periodic repeat revealing the channels traversing through the porous structure with sphere model and polyhedral rendering of the atom positions, (c) atomistic structure of a small segment in part b, (d) schematic of the Mn polyhedra revealing the 1 × 1 tunnels along which (*c*-direction) the Li ions move. We denote "channels" as the large (cavity) interconnects that exist at a hierarchical length scale above "tunnels"; the latter exist as a consequence of the polymorphic crystal structure.

(27) Tang, W. P.; Yang, X. J.; Liu, Z. H.; Ooi, K. *J. Mater. Chem.* **2003**, *13*, 2989–2995.

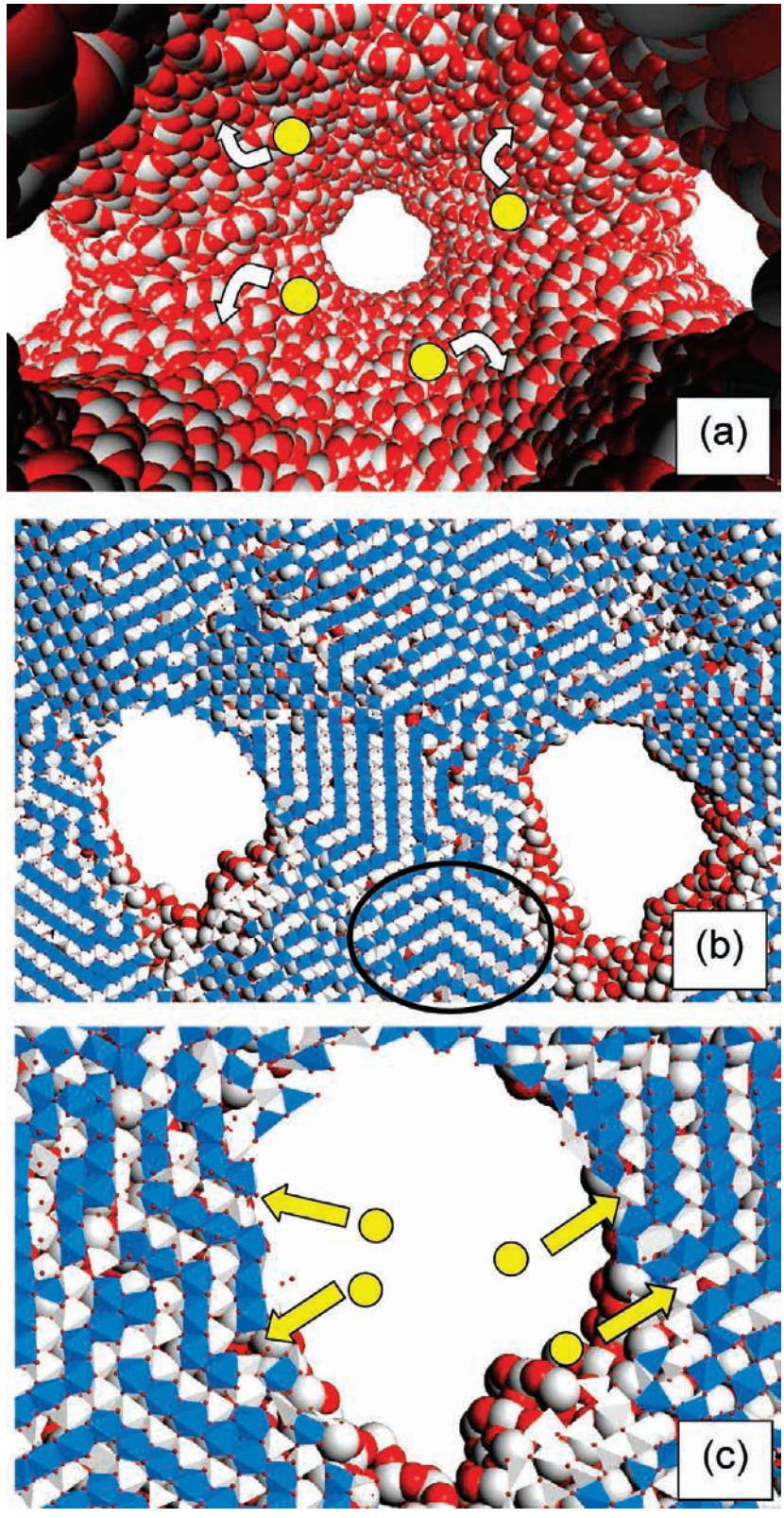

Figure 13. Models of the atom positions showing the internal pores and connecting channels comprising the nanoporous MnO_2: (a) perspective view showing an internal pore and connecting channels, sphere model representation of the atom positions; (b) slice cut through the MnO_2 revealing the microtwinning, an example is highlighted by the black oval; (c) enlarged segment of part b showing more clearly the positions (yellow arrows) that the Li ions can insert into the surface of the MnO_2 host via 1×1 tunnels. Mn plane atoms above the page are colored blue; polyhedra below the page are white to reveal more clearly the 1×1 tunnels. Oxygen is red, manganese is white, and lithium is yellow. Li ions are shown as schematic.

wall thickness of the channels is inextricably linked with the depth of discharge. Specifically, a deeper discharge reduces the critical thickness. Accordingly, if one is to optimize the electrochemical properties (maximize charge capacity and retain structural integrity during cycling) one needs to minimize the wall thickness.

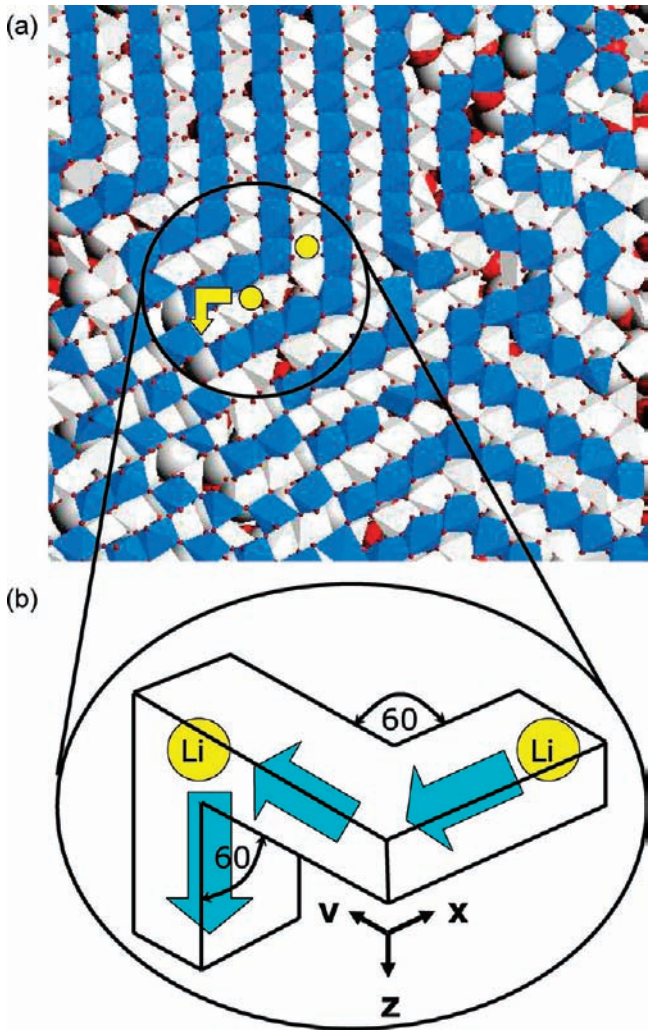

Figure 14. Atomistic model and schematic illustrating the 3D mobility of Li in nanoporous MnO_2 (Li atoms are schematic): (a) atomistic model showing the 1×1 tunnels, (b) schematic showing how the Li can move in all three spacial directions in the porous MnO_2.

We propose also that the considerable twinning that we observe in our structural model enables Li to insert anywhere on the internal surface and move spatially in all three directions. This will facilitate an even expansion of the framework upon insertion/deinsertion and thus enable the material to expand elastically and protect against plastic deformation upon cycling. However, an even expansion necessitates that the porous material be periodic. For example, if one region were larger than its neighbor, then it could accommodate a higher concentration of Li and thus expand more. A discontinuity in expansion would impose higher stress at a particular point and, if sufficiently high, would lead to plastic deformation. This argument is supported by experimental data from Lai and coworkers who found that the stress−strain curve for porous copper with a periodic (P) minimal surface structure revealed a higher elastic modulus and yield stress compared with its nonperiodic porous counterpart.[6] They attributed this observation to a *uniform* force distribution over the material during compression. Consequently, high forces, which might result in deformation of the nanoporous structure via plastic collapse, were not focused at specific points.

We also suggest tentatively that our predictions for MnO_2 are more general in that they apply to other nanomaterials, such as rutile TiO_2, which can expand and contract elastically rather than plastically, upon charging/discharging.

Conclusions

The properties of a nanomaterial can be fine-tuned or new properties proffered compared to the parent (bulk) material "simply" by changing the size of one or more dimensions in the nanometer range. However, populating (nano)structure−property correlation tables, which will prove invaluable in the intelligent design of new nanomaterials, necessitates characterization of the nanostructure with atomistic detail. This is difficult experimentally, and therefore, atomistic computer simulation offers a unique window of exploration into such materials. Conversely, while approaches to generate atomistic models for crystal structures are well developed and have been widely used for over 60 years,[19,20] analogous systematic approaches for generating atomistic models for nanostructures are not yet available. Here, we develop and use a systematic strategy for generating full atomistic models for nanomaterials, spanning all spatial dimensions including the following: nanoparticle (0D), nanorod (1D), nanosheet (2D), and nanoporous structure (3D).

Atomistic models for a crystal are normally generated by constructing a simulation cell and positioning (model) atoms at basis positions: the symmetry is then used to replicate the crystal infinitely in space using periodic boundary conditions. We show how model nanostructures can be prescribed by exploiting the symmetry and lattice parameters associated with the nanostructure and positioning nanoparticles (rather than atoms) at basis positions. This strategy, analogous to that for generating crystal structures, enables a systematic approach for the generation of model nanomaterials. The particular polymorphic crystal structure is facilitated via simulated amorphization and crystallization.

We test the approach by generating models of MnO_2 nanostructures, which is an important material with respect to energy storage; mesoporous β-MnO_2 can be used as a reversible positive electrode in rechargeable Li ion batteries. We find a close analogy between experiment and model at three levels of hierarchical structural complexity: (i) crystal structure (β-MnO_2 polymorph), (ii) microstructure (microtwinning, grain boundaries, point defects), and (iii) nanostructure (particle, rod, sheet, porous structure) thus validating the approach.

In its capacity as a component in a rechargeable battery, Li ions must be easily inserted, stored, and deinserted into MnO_2, which acts as a host lattice. Our atomistic models are valuable in that one can explore the models at the atomistic level to observe the openings of the tunnels, deep inside the nanopores, into which Li inserts. Such regions are notoriously difficult to explore experimentally, and therefore, simulation can provide valuable and unique insight. In particular, we found that the microtwinning in the MnO_2 host lattice enables Li insertion at almost any position on the internal surface of the nanoporous MnO_2 and facilitates Li transport in all three spatial directions in the material. This enables the MnO_2 to expand and contract linearly under charge/discharge cycles. Accordingly, the stress is evenly distributed, and the material can expand/contract elastically. Uneven forces would likely lead to plastic deformation resulting in electrochemical property fading during cycling.

We propose also that there exists a "critical (wall) thickness" for "nano" architectures above which Li insertion is accommodated via a plastic, rather than elastic, deformation of the host lattice leading to fading of its energy storage capacity upon cycling, and we propose that this critical thickness is dependent

upon the depth of discharge. Accordingly, to maximize the charge capacity ("depth of discharge"), one needs to reduce (minimize) the wall thickness to below its critical thickness. We propose that this prediction may help explain why certain forms of MnO_2 are electrochemically active, while others are not.

Acknowledgment. This work is based upon the research supported by the South African Research Chair Initiative of the Department of Science and Technology and the National Research Foundation and the Centre for High Performance Computing (CHPC) in South Africa.

Supporting Information Available: Discussion of simulated amorphization and recrystallization strategy. This material is available free of charge via the Internet at http://pubs.acs.org.

JA8082335